Transforming Space with Non-Hermitian Dielectrics

Ivor Krešić,[1,2,*] Konstantinos G. Makris,[3,4] Ulf Leonhardt,[5] and Stefan Rotter[1]
[1]Institute for Theoretical Physics, Vienna University of Technology (TU Wien), Vienna A-1040, Austria
[2]Institute of Physics, Bijenička cesta 46, 10 000 Zagreb, Croatia
[3]ITCP-Physics Department, University of Crete, Heraklion 71003, Greece
[4]Institute of Electronic Structure and Lasers (IESL), Foundation for Research and Technology–Hellas, Heraklion 71110, Greece
[5]Department of Physics of Complex Systems, Weizmann Institute of Science, Rehovot 761001, Israel

(Received 24 November 2021; accepted 14 April 2022; published 4 May 2022)

Coordinate transformations are a versatile tool to mold the flow of light, enabling a host of astonishing phenomena such as optical cloaking with metamaterials. Moving away from the usual restriction that links isotropic materials with conformal transformations, we show how nonconformal distortions of optical space are intimately connected to the complex refractive index distribution of an isotropic non-Hermitian medium. Remarkably, this insight can be used to circumvent the material requirement of working with refractive indices below unity, which limits the applications of transformation optics. We apply our approach to design a broadband unidirectional dielectric cloak, which relies on nonconformal coordinate transformations to tailor the non-Hermitian refractive index profile around a cloaked object. Our insights bridge the fields of two-dimensional transformation optics and non-Hermitian photonics.

DOI: 10.1103/PhysRevLett.128.183901

The introduction of coordinate transformations into optics has enabled a host of interesting applications such as optical cloaking—the ability of a device to conceal an object by shielding it from interacting with the incoming light [1,2]. However, the early designs of optical cloaks were hindered by demanding requirements, which prompted the search for materials with unconventional properties [3]. Although this search continues today, some of these requirements, such as a vanishing refractive index, anisotropy, or a nonvanishing magnetic susceptibility, have been found to come with severe restrictions such as a spectrally narrow optical response window. In spite of great efforts to circumvent these obstacles [4–10], some applications like stand-alone cloaks [1,2,11] still rely on such properties.

On another seemingly unrelated front, that of non-Hermitian photonics [12–19], engineering the imaginary part of the index of refraction has led to a plethora of experimental demonstrations [20–28] with various novel applications [29–32]. Gain and loss provides an extra degree of freedom (different from negative or anisotropic electromagnetic responses) which offers an alternative route for controlling the flow of light with a non-Hermitian medium.

In this Letter we demonstrate how transformation optics and the engineering of non-Hermitian media can be directly linked. Specifically, in isotropic materials the nonconformal transformations naturally lead to spatially modulated gain and loss. When using them for constructing an invisibility cloak, such materials not only bend the phase fronts of light around the cloaked object, but the involved gain and loss distribution also provides sources and sinks for the probing light field. This can be used for designing a unidirectional broadband non-Hermitian version of the Zhukovsky cloak [1,33,34]. Rather than featuring anisotropic [2], epsilon near zero (ENZ) [35,36], or negative index [37,38] materials, this non-Hermitian cloak just consists of a dielectric isotropic medium with spatially modulated gain and loss. With the underlying strategy to use nonconformal maps to design non-Hermitian index landscapes, we also open up new directions for the application of transformation optics in general. We envision, for example, that based on our results many of the existing conformal mapping setups in two-dimensional (2D) media [34] could also be considered for potential nonconformal extensions. The resulting non-Hermitian distributions can then be experimentally implemented with a spatially modulated pump beam [39–41].

Our starting point is the Helmholtz equation that describes the scattering of a linearly polarized electric field of a given wavelength λ_0 at a 2D isotropic material landscape. Following the strategy of transformation optics, we first consider a "virtual space" with coordinates (x', y'), in which the incoming light sees a homogeneous medium with a constant and real refractive index n_0. The corresponding Helmholtz equation is given as follows:

$$\Delta' E(x', y') + n_0^2 k_0^2 E(x', y') = 0, \tag{1}$$

where $\Delta' = \nabla'^2 = \partial^2/\partial x'^2 + \partial^2/\partial y'^2$, with $k_0 = 2\pi/\lambda_0$. We now translate this equation to "physical space" to obtain a transformed Helmholtz equation that features the

same field distribution E in the physical coordinates (x, y) and in the inhomogeneous (but isotropic) refractive index landscape $n^2(x, y)$:

$$\Delta E(x, y) + n^2(x, y)k_0^2 E(x, y) = 0, \tag{2}$$

where $\Delta = \nabla^2 = \partial^2/\partial x^2 + \partial^2/\partial y^2$. If we do not restrict ourselves to conformal (i.e., angle-preserving) transformations, the refractive index $n(x, y) = n_R(x, y) + in_I(x, y)$, which is now a complex-valued function in general, satisfies the following complicated relation that notably depends not only on the virtual index n_0 and the coordinate transformation $[x'(x, y), y'(x, y)]$, but also on the specific solution $E(x', y')$ in virtual space [see the Supplemental Material (SM) for details [42]]:

$$n^2(x, y) = \frac{n_0^2}{2}[(\nabla x')^2 + (\nabla y')^2] - \frac{1}{k_0^2}\left(\Delta x' \frac{\partial \ln E}{\partial x'} + \Delta y' \frac{\partial \ln E}{\partial y'}\right) - \frac{2}{k_0^2}(\nabla x' \cdot \nabla y')\left(\frac{\partial^2 \ln E}{\partial x' \partial y'} + \frac{\partial \ln E}{\partial x'}\frac{\partial \ln E}{\partial y'}\right)$$
$$- \frac{1}{2k_0^2}[(\nabla x')^2 - (\nabla y')^2]\left[\frac{\partial^2 \ln E}{\partial x'^2} + \left(\frac{\partial \ln E}{\partial x'}\right)^2 - \frac{\partial^2 \ln E}{\partial y'^2} - \left(\frac{\partial \ln E}{\partial y'}\right)^2\right]. \tag{3}$$

Whereas the first term on the right-hand side of the above equation, $(n_0^2/2)[(\nabla x')^2 + (\nabla y')^2]$, is the conformal part (see, e.g., Ref. [33]), the remaining terms stem from the nonconformality of on the coordinate transformation. Since these new terms bind the transformation of the index to a certain solution in virtual space, $E(x', y')$, they appear very impractical at first glance. It turns out, however, that for the canonical case of a plane-wave input in positive x direction, corresponding to a virtual solution $E(x', y') = E_0 e^{in_0 k_0 x'}$, the optical potential in real space drastically simplifies to take the intensity-independent form:

$$n^2(x, y) = n_0^2\left[(\nabla x')^2 - \frac{i}{n_0 k_0}\Delta x'\right]. \tag{4}$$

Remarkably, this expression for $n^2(x, y)$ is equivalent to the 2D constant-intensity (CI) potential that has recently been studied extensively [43–51] (see the SM [42]). CI waves are a special solution of the Helmholtz equation for which a judiciously chosen modulation of gain and loss suppresses wave scattering entirely. Moreover, as was recently shown in Refs. [48,50], the media supporting such waves can be made unidirectionally invisible for a broad range of input frequencies. With Eq. (4) we have thus discovered that CI waves in physical space arise naturally through a nonconformal coordinate transformation of the plane-wave solution in homogeneous virtual space. This provides a simple geometrical interpretation of CI waves, and some of their hitherto unexplained properties, such as their robustness to frequency detuning, can be seen as a direct consequence of this interpretation.

In 2D virtual space not only plane waves but also other continuous wave solutions can be identified, for which the refractive index of Eq. (3) will be independent of the virtual beam's intensity. Such solutions typically have separable amplitude-dependent and amplitude-independent parts, another example of which is a Gaussian beam. On the other hand, electric field solutions with diverging logarithmic derivatives, such as Bessel [52] and Airy beams [53], will create regions of infinite $n(x, y)$, and are hence unsuitable for our transformation protocol.

We now apply the above approach to a well-studied example in the literature on transformation optics, which is the Zhukovsky map [54] that has been used extensively in conformal transformation optics for the design of invisibility cloaks [1,33,34]. We start with the expression for the conformal Zhukovsky map, $w_{\mathrm{Zh}}(z) = z + 1/z$, where we have used the convenient notation $w = x' + iy'$ for the virtual coordinates, and $z = x + iy$ for the physical coordinates [note that (x', y') and (x, y) are real valued; see Refs. [55–57] for examples of complex-valued transformations]. Illustrations of the conformal Zhukovsky transformation are provided in Figs. 1(a) and 1(b): the light green line in virtual space, see Fig. 1(a) (branch cut connecting the points $w = \pm 2$), is transformed into the light green unit circle in physical space, see Fig. 1(b). A plane wave traveling in positive x direction of virtual space will thus be guided around the cloak boundary, placed right at this circle in physical space. Importantly for the present case, the conformal Zhukovsky map features two points located at $z = \pm 1$, right at the cloak boundary, where the refractive index in physical space vanishes [see light green points in Fig. 1(b) and dark blue parts in Fig. 2(a)]. The cloak thus requires the use of materials with a vanishing refractive index, which limits the cloak functionality to narrow-band radiation.

With the approach presented above, such limitations can be conveniently circumvented through the use of nonconformal maps that naturally lead to non-Hermitian materials with complex refractive profiles. In particular, to design such a non-Hermitian cloak, we modify the Zhukovsky map as $w(z, z^*) = z + \eta(z, z^*)/z$.

In contrast to the conformal map $w_{\mathrm{Zh}}(z)$, the map $w(z, z^*)$ depends on both z and its complex conjugate z^*, which violates conformality [compare Figs. 1(b) and 1(c)]. In the present case, we choose the envelope

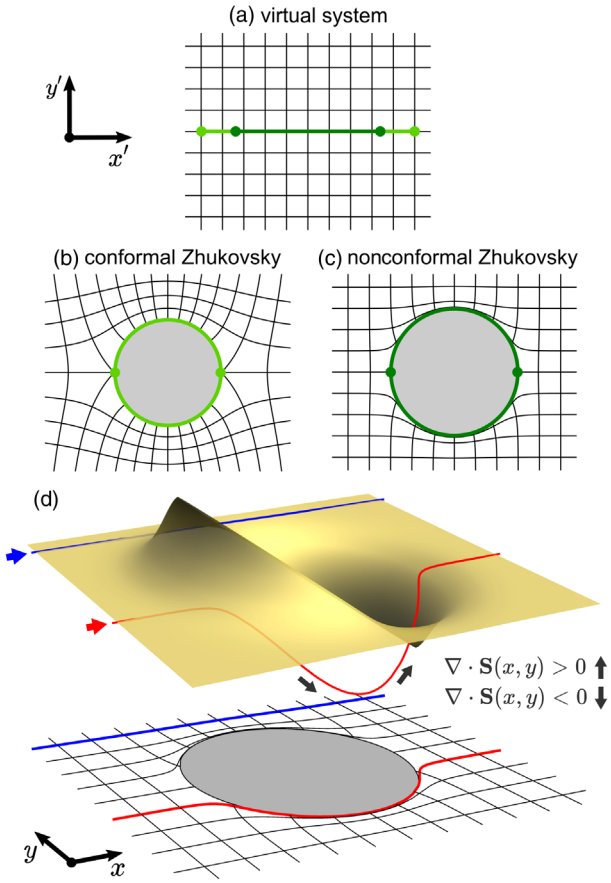

FIG. 1. Transforming space with non-Hermitian media. (a) The virtual coordinates, with the branch cuts of the conformal (light green) and nonconformal (dark green) Zhukovsky maps. The area of each square in the grid is 0.4×0.4. After the mappings, the green lines form circles, see (b) and (c), inside of which is the cloaked region (gray shaded area). The local orthogonality of the coordinate lines, a signature of conformal mapping, is present only in (b) but not in (c) (in both plots only the upper Riemann sheet is depicted). (d) Visualization of light propagation in the proposed non-Hermitian cloak profile, with the blue and red lines being the equivalent of rays in a non-Hermitian landscape (see the SM [42]). The yellow surface indicates the imaginary part of the dielectric function, that causes the blue and red lines to rise or fall in the direction orthogonal to the x-y plane, indicating the local creation $[\nabla \cdot \mathbf{S}(x, y) > 0]$ or destruction $[\nabla \cdot \mathbf{S}(x, y) < 0]$ of energy flux. The projection of the lines onto the 2D plane coincides with the inversely transformed coordinates, plotted in the grid below, with the cloaked region shaded in gray.

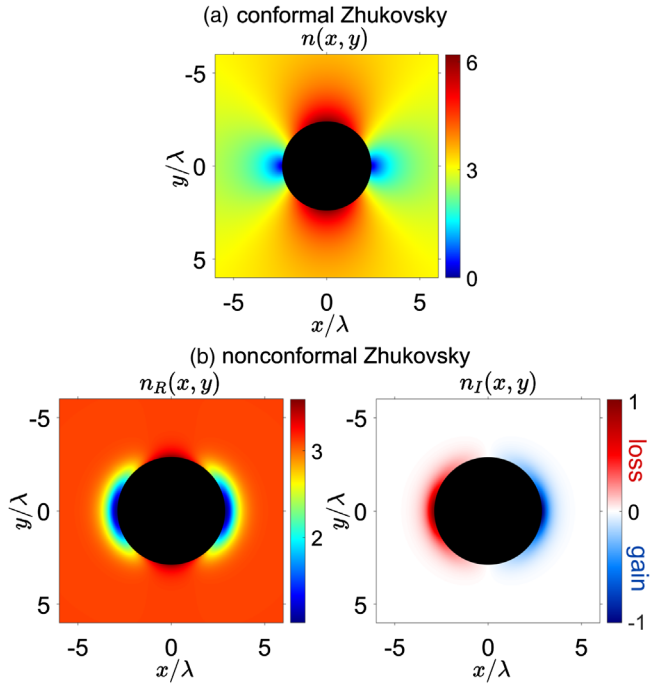

FIG. 2. Refractive index distributions for the conformal and nonconformal Zhukovsky cloaks. (a) Real-valued refractive index distribution of the conformal Zhukovsky cloak, reaching values of $n = 0$ at $x = \pm 2.4\lambda$, and requiring the use of ENZ materials. Here, $\lambda = \lambda_0/n_0$ and $n_0 = 3.1$. (b) Real (left) and imaginary (right) parts of the refractive index spatial profile of the nonconformal Zhukovsky map. The refractive index based on Eq. (4) is calculated using the transformation $w(z, z^*)$ with $\eta(z, z^*) = 1/[1 + e^{\beta(|z|-R_1)}] - 1/[1 + e^{\beta(|z|-R_0)}]$ and $R_0 = 0.25$, $R_1 = 1$, $\beta = 5.75$. The values for $n_R(x, y)$ lie between 1.013 and 3.594, whereas those of $n_I(x, y)$ lie between -1.013 and 1.013. The black filled circle in all panels indicates the cloaked region.

$\eta(z, z^*)$ as a function of $|z|$ to have the shape of a flattop function with smoothed edges (see caption of Fig. 2). For large values of $|z| \gg 1$ the envelope $\eta(z, z^*)$ vanishes $[w(z, z^*) \to z]$, while at $|z| \approx 1$ it has an edge with finite first and second derivatives, such that the vanishing of n_R at $x = \pm 1 = \pm 2.4\lambda$, shown for the conformal Zhukovsky map in Fig. 2(a), is avoided, according to Eq. (4). We have found that for a judicious choice of $\eta(z, z^*)$ excellent cloaking can be achieved when the cloak's outer radius corresponds to the radius of the branch cut in physical space. For the cloak we show here, this radius is $|z| = 1.20458 = 2.86\lambda$, and is indicated by the dark green line and circle in Figs. 1(a) and 1(c), respectively. The resulting material is dielectric with $n_R(x, y) = \mathrm{Re}[n(x, y)] > 1$ in all points of physical space, but with an inhomogeneous gain-loss distribution, given by $n_I(x, y) = \mathrm{Im}[n(x, y)]$.

The principle of the cloak's operation is schematically depicted in Fig. 1(d). The yellow surface represents the imaginary part of the dielectric profile, $\varepsilon_I(x, y) = \mathrm{Im}[n^2(x, y)]$. As the energy flux is created and destroyed in regions of gain and loss, the representation of light as rays in 2D space is not appropriate in non-Hermitian media. To visualize the light propagation, we plot instead the lines whose increase (decrease) in the direction orthogonal to the x-y plane marks the creation (destruction) of the Poynting flux $\mathbf{S}(x, y)$ (see the SM [42]). The cloaking for a beam incoming from the negative x direction [red line in the upper plot of Fig. 1(d)] can be explained by the interplay of the real and imaginary parts of the refractive index

distribution, which form here a parity-time- (PT) symmetric system [see Fig. 2(b)]. The part of the beam that is sufficiently displaced from the cloak center (blue line) sees a noncurved space, and propagates in a straight line in the homogeneous background medium. For beam parts near the center (red line), similarly to the conformal Zhukovsky mapping, the real part of the refractive index distribution works to bend the light around the object. Since, however, we have $n_R > 1$ in all of physical space, the real part of the refractive index alone is insufficient to achieve the cloaking effect: in fact, the finite imaginary part of the refractive index distribution partially absorbs the incoming electric field [$\nabla \cdot \mathbf{S}(x, y) < 0$] in front of the cloak and amplifies it [$\nabla \cdot \mathbf{S}(x, y) > 0$] behind the cloak.

To demonstrate the cloaking efficiency, we solve Eq. (2) with $n(x, y)$ of Fig. 2(b) numerically by using the open source finite-element solver NGSolve [58,59]. Inside of the cloaked region that we terminate with a Neumann boundary condition in physical space, we place a highly reflective material with a circular cross section. Choosing the background value of the refractive index in virtual space as $n_0 = 3.1$, we find that $n_R(x, y)$ varies between 1.013 and 3.594, whereas $n_I(x, y)$ has values between ± 1.013. In the SM, we also show the results for an alternative parameter regime, where the cloak region has a smaller radius but the $n_I(x, y)$ varies with an amplitude as low as ± 0.08 [42].

When the cloak is present [Fig. 3(a)], the beam incoming from the left is perfectly transmitted to the right side, with both phase and amplitude in the far field being equal to that of a plane wave in virtual space with a refractive index n_0

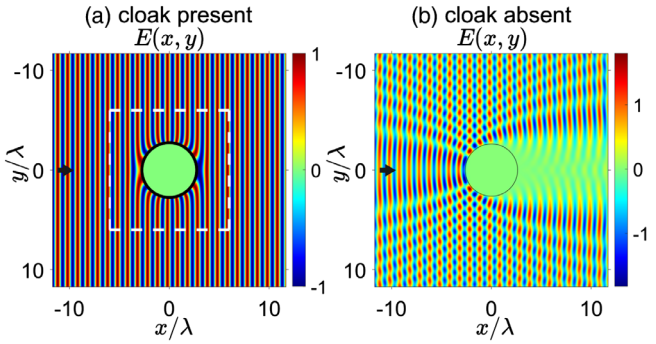

FIG. 3. Non-Hermitian cloaking for an incoming plane wave at the central design spatial frequency $k = n_0 k_0$. (a) Electric field solution for the case when cloaking is present. The refractive index distribution is that of Fig. 2(b), with the dashed white box denoting the area plotted there. The black ring represents the annulus of the cloak, where the Neumann boundary condition of vanishing normal electric field derivative was used. Inside the annulus there is a highly reflective material, taken here as aluminum ($n_{\mathrm{Al}} = 1.52 + 9.26i$ at 1 μm [60]), with a circular cross section. (b) The electric field solution for the same incoming field but with only the highly reflective material present. The cloak's outer radius is 2.86λ, while its inner radius is 2.62λ. The fields are normalized to the incoming wave amplitude. The black arrow marks the propagation direction of the incoming beam.

(see also Fig. S2 of the SM [42]). Inside the cloaked area, the field completely vanishes, as expected. When the cloak is absent [Fig. 3(b)], strong scattering occurs and a shadow is formed behind the cloak.

Concerning the directional sensitivity of the cloak operation, we recall that already the conformal Zhukovsky cloak is sensitive to changes of the incidence angle with respect to the normal axis (see the SM [42]). The cloak in Fig. 2(b) retains a similar sensitivity to such deviations, with an appreciable reduction of efficiency already at input beam tilts of around $\pm 2°$ to the normal, making the cloaking effectively unidirectional.

To put these results in the context of previous theoretical work, let us mention here Ref. [61], where a cloak based on anisotropic non-Hermitian electric and magnetic materials was designed by transforming a PT-symmetric potential in the virtual coordinates to the physical space—an idea later transferred also to acoustics [62]. In a similar vein, folding and stretching of non-Hermitian virtual space has recently been used to construct 2D gain-loss distributions that are robustly balanced [63]. In Ref. [64], a cloaking strategy based on subwavelength layers of balanced gain and loss was devised, using conducting non-Hermitian metamaterials with locally infinite reflection coefficients. This strategy, although similar in spirit to active cloaking, does not require the knowledge of the input wave properties for successful cloak operation, in contrast to the earlier work of Refs. [65,66]. We note here that none of the earlier non-Hermitian cloaking work, that we are aware of, involves transformation optics with isotropic dielectric media, as we do in this Letter. The first remarkable successes in the direction of non-Hermitian transformation optics were made in one-dimensional (1D) systems, using complex spatial coordinates [55–57].

A notable disadvantage afflicting ENZ [1], anisotropic [11], and layered non-Hermitian cloaks [64] alike is the requirement of extreme real refractive index values (or admittance values [64]), which limits the cloak's operation to frequencies near metamaterial resonances. As our cloak features inhomogeneous dielectric media with $n_R > 1$ and finite values of n_I, which are known to have reasonably fast and frequency-broadband responses (see, e.g., Refs. [67,68]), we now investigate the behavior of our cloak under pulsed illumination.

Strictly speaking, the cloak's refractive index distribution in Eq. (4) should produce its desired effect only at the design wave number $k = n_0 k_0$. Perfect cloaking from pulsed radiation would thus require the tailoring of not only the spatial but also the frequency dependence of the refractive index distribution. We choose here to approximate the spectral index distribution to be entirely frequency independent in the k range of the input pulse, while using the spatial distribution shown in Fig. 2(b). The results, shown in Fig. 4(a), demonstrate excellent cloaking performance for pulses with a spectral width of $\sigma_k = 0.055k$, thereby confirming the robustness of the design in Eq. (4) to frequency detuning.

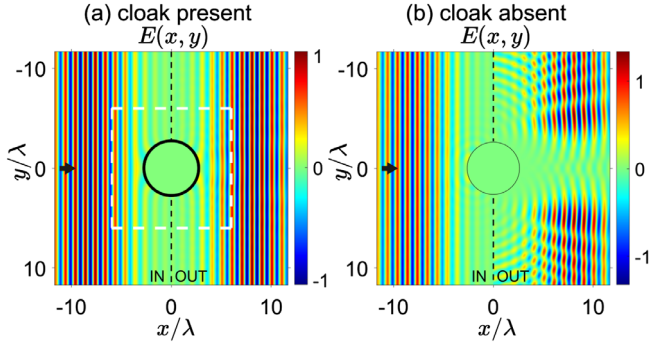

FIG. 4. Demonstration of cloaking under pulsed illumination, for the optical media as in Fig. 3. (a) A spatially narrow pulse incident onto the cloaking region (left) is nearly perfectly transmitted (right) when the cloak is present. (b) When the cloak is absent, there is a distortion of the pulse shape, clearly revealing the presence of the reflecting material ($n_{\mathrm{Al}} = 1.52 + 9.26i$) to the outside observer. The thin black dashed line denotes the separation of the plotting regions for the incoming (left) and outgoing (right) part of the pulse evolution; all other markings are as in Fig. 3. The time evolution was calculated by an inverse Fourier transform, using a Gaussian envelope with a width of $\sigma_k = 0.055k$ in k space.

To summarize, we have introduced a new way to achieve optical cloaking in dielectric systems without using ENZ or anisotropic materials, and demonstrated that nonconformal maps naturally lead to complex isotropic indices of refraction. Based on a nonconformal Zhukovsky transformation, a non-Hermitian invisibility cloak is introduced, which also works for incoming pulses. We note that our transformation optics design is fully analytical, but still optimization strategies could also be applied in order to optimize the corresponding refractive index profiles, with relatively low computational effort as compared to previous work in non-Hermitian optimization problems [39–41]. Although the discussed synergy between non-Hermitian photonics and 2D isotropic transformation optics is expected to lead to many more interesting insights, we emphasize here that it should be possible to extend our theoretical methodology to three spatial dimensions, where the vectorial properties of light-matter interaction play a significant role.

The work of I. K. was funded by the Austrian Science Fund (FWF) Lise Meitner Postdoctoral Fellowship M3011 and the FWF Grant No. P32300. The joint work of I. K., K. G. M., and S. R. was supported by the European Commission Grant No. MSCA-RISE 691209. U. L. was supported by the Israel Science Foundation and the Murray B. Koffler Professorial Chair. The computational results presented here have been obtained using the Vienna Scientific Cluster (VSC).

*ivor.kresic@tuwien.ac.at

[1] U. Leonhardt, Science **312**, 1777 (2006).
[2] J. B. Pendry, D. Schurig, and D. R. Smith, Science **312**, 1780 (2006).
[3] H. Chen, C. T. Chan, and P. Sheng, Nat. Mater. **9**, 387 (2010).
[4] J. Li and J. B. Pendry, Phys. Rev. Lett. **101**, 203901 (2008).
[5] J. Valentine, J. Li, T. Zentgraf, G. Bartal, and X. Zhang, Nat. Mater. **8**, 568 (2009).
[6] L. H. Gabrielli, J. Cardenas, C. B. Poitras, and M. Lipson, Nat. Photonics **3**, 461 (2009).
[7] T. Ergin, N. Stenger, P. Brenner, J. B. Pendry, and M. Wegener, Science **328**, 337 (2010).
[8] X. Ni, Z. J. Wong, M. Mrejen, Y. Wang, and X. Zhang, Science **349**, 1310 (2015).
[9] L. Hsu, T. Lepetit, and B. Kante, Prog. Electromagn. Res. **152**, 33 (2015).
[10] M. McCall, J. B. Pendry, V. Galdi, Y. Lai, S. Horsley, J. Li, J. Zhu, R. C. Mitchell-Thomas, O. Quevedo-Teruel, P. Tassin *et al.*, J. Opt. **20**, 063001 (2018).
[11] D. Schurig, J. J. Mock, B. J. Justice, S. A. Cummer, J. B. Pendry, A. F. Starr, and D. R. Smith, Science **314**, 977 (2006).
[12] K. G. Makris, R. El-Ganainy, D. N. Christodoulides, and Z. H. Musslimani, Phys. Rev. Lett. **100**, 103904 (2008).
[13] Z. Lin, H. Ramezani, T. Eichelkraut, T. Kottos, H. Cao, and D. N. Christodoulides, Phys. Rev. Lett. **106**, 213901 (2011).
[14] Y. D. Chong, L. Ge, H. Cao, and A. D. Stone, Phys. Rev. Lett. **105**, 053901 (2010).
[15] S. Longhi, Europhys. Lett. **120**, 64001 (2017).
[16] R. El-Ganainy, K. G. Makris, M. Khajavikhan, Z. H. Musslimani, S. Rotter, and D. N. Christodoulides, Nat. Phys. **14**, 11 (2018).
[17] S. K. Özdemir, S. Rotter, F. Nori, and L. Yang, Nat. Mater. **18**, 783 (2019).
[18] M.-A. Miri and A. Alú, Science **363**, eaar7709 (2019).
[19] S. Yao and Z. Wang, Phys. Rev. Lett. **121**, 086803 (2018).
[20] C. E. Rüter, K. G. Makris, R. El-Ganainy, D. N. Christodoulides, M. Segev, and D. Kip, Nat. Phys. **6**, 192 (2010).
[21] A. Regensburger, C. Bersch, M.-A. Miri, G. Onishchukov, D. N. Christodoulides, and U. Peschel, Nature (London) **488**, 167 (2012).
[22] L. Feng, Y.-L. Xu, W. S. Fegadolli, M.-H. Lu, J. E. B. Oliveira, V. R. Almeida, Y.-F. Chen, and A. Scherer, Nat. Mater. **12**, 108 (2013).
[23] B. Peng, S. K. Özdemir, F. Lei, F. Monifi, M. Gianfreda, G. L. Long, S. Fan, F. Nori, C. M. Bender, and L. Yang, Nat. Phys. **10**, 394 (2014).
[24] B. Peng, S. K. Özdemir, S. Rotter, H. Yilmaz, M. Liertzer, F. Monifi, C. M. Bender, F. Nori, and L. Yang, Science **346**, 328 (2014).
[25] L. Feng, Z. J. Wong, R.-M. Ma, Y. Wang, and X. Zhang, Science **346**, 972 (2014).
[26] H. Hodaei, M.-A. Miri, M. Heinrich, D. N. Christodoulides, and M. Khajavikhan, Science **346**, 975 (2014).
[27] J. Doppler, A. A. Mailybaev, J. Böhm, U. Kuhl, A. Girschik, F. Libisch, T. J. Milburn, P. Rabl, N. Moiseyev, and S. Rotter, Nature (London) **537**, 76 (2016).
[28] S. Weidemann, M. Kremer, T. Helbig, T. Hofmann, A. Stegmaier, M. Greiter, R. Thomale, and A. Szameit, Science **368**, 311 (2020).

[29] S. Assawaworrarit, X. Yu, and S. Fan, Nature (London) **546**, 387 (2017).
[30] K. Pichler, M. Kühmayer, J. Böhm, A. Brandstötter, P. Ambichl, U. Kuhl, and S. Rotter, Nature (London) **567**, 351 (2019).
[31] Z. Zhang, X. Qiao, B. Midya, K. Liu, J. Sun, T. Wu, W. Liu, R. Agarwal, J. M. Jornet, S. Longhi, N. M. Litchinitser, and L. Feng, Science **368**, 760 (2020).
[32] S. Xia, D. Kaltsas, D. Song, I. Komis, J. Xu, A. Szameit, H. Buljan, K. G. Makris, and Z. Chen, Science **372**, 72 (2021).
[33] U. Leonhardt and T. Philbin, *Geometry and Light: The Science of Invisibility* (Courier Corporation, Mineola, 2010).
[34] L. Xu and H. Chen, Nat. Photonics **9**, 15 (2015).
[35] A. Alú, M. G. Silveirinha, A. Salandrino, and N. Engheta, Phys. Rev. B **75**, 155410 (2007).
[36] P. Moitra, Y. Yang, Z. Anderson, I. I. Kravchenko, D. P. Briggs, and J. Valentine, Nat. Photonics **7**, 791 (2013).
[37] J. B. Pendry, Phys. Rev. Lett. **85**, 3966 (2000).
[38] J. Valentine, S. Zhang, T. Zentgraf, E. Ulin-Avila, D. A. Genov, G. Bartal, and X. Zhang, Nature (London) **455**, 376 (2008).
[39] N. Bachelard, J. Andreasen, S. Gigan, and P. Sebbah, Phys. Rev. Lett. **109**, 033903 (2012).
[40] T. Hisch, M. Liertzer, D. Pogany, F. Mintert, and S. Rotter, Phys. Rev. Lett. **111**, 023902 (2013).
[41] N. Bachelard, S. Gigan, X. Noblin, and P. Sebbah, Nat. Phys. **10**, 426 (2014).
[42] See Supplemental Material at http://link.aps.org/supplemental/10.1103/PhysRevLett.128.183901 for a derivation of Eqs. (3) and (4), and details on the visualization of beam propagation shown in Fig. 1(d), thick cloak regime and beam incidence angle scans.
[43] K. G. Makris, Z. H. Musslimani, D. N. Christodoulides, and S. Rotter, Nat. Commun. **6**, 7257 (2015).
[44] K. G. Makris, A. Brandstötter, P. Ambichl, Z. H. Musslimani, and S. Rotter, Light Sci. Appl. **6**, e17035 (2017).
[45] S. Yu, X. Piao, and N. Park, Phys. Rev. Lett. **120**, 193902 (2018).
[46] E. Rivet, A. Brandstötter, K. G. Makris, H. Lissek, S. Rotter, and R. Fleury, Nat. Phys. **14**, 942 (2018).
[47] P. Sebbah, Nat. Photonics **11**, 337 (2017).
[48] A. Brandstötter, K. G. Makris, and S. Rotter, Phys. Rev. B **99**, 115402 (2019).
[49] S. A. R. Horsley, Phys. Rev. A **100**, 053819 (2019).
[50] K. G. Makris, I. Krešić, A. Brandstötter, and S. Rotter, Optica **7**, 619 (2020).
[51] A. F. Tzortzakakis, K. G. Makris, S. Rotter, and E. N. Economou, Phys. Rev. A **102**, 033504 (2020).
[52] J. Durnin, J. J. Miceli, and J. H. Eberly, Phys. Rev. Lett. **58**, 1499 (1987).
[53] G. A. Siviloglou, J. Broky, A. Dogariu, and D. N. Christodoulides, Phys. Rev. Lett. **99**, 213901 (2007).
[54] N. E. Zhukovsky, Z. Flugtech. Motorluftschiff. **1**, 281 (1912).
[55] G. Castaldi, S. Savoia, V. Galdi, A. Alú, and N. Engheta, Phys. Rev. Lett. **110**, 173901 (2013).
[56] S. A. R. Horsley, C. G. King, and T. G. Philbin, J. Opt. **18**, 044016 (2016).
[57] S. Savoia, G. Castaldi, and V. Galdi, J. Opt. **18**, 044027 (2016).
[58] J. Schöberl, Comput. Visualization Sci. **1**, 41 (1997).
[59] J. Schöberl, ASC Report 30/2014, Institute for Analysis and Scientific Computing, Vienna University of Technology, 2014.
[60] A. D. Rakić, A. B. Djurišić, J. M. Elazar, and M. L. Majewski, Appl. Opt. **37**, 5271 (1998).
[61] X. Zhu, L. Feng, P. Zhang, X. Yin, and X. Zhang, Opt. Lett. **38**, 2821 (2013).
[62] X. Zhu, H. Ramezani, C. Shi, J. Zhu, and X. Zhang, Phys. Rev. X **4**, 031042 (2014).
[63] L. Luo, J. Luo, H. Chu, and Y. Lai, Adv. Photonics Res. **2**, 2000081 (2021).
[64] D. L. Sounas, R. Fleury, and A. Alú, Phys. Rev. Applied **4**, 014005 (2015).
[65] D. A. B. Miller, Opt. Express **14**, 12457 (2006).
[66] M. Selvanayagam and G. V. Eleftheriades, Phys. Rev. X **3**, 041011 (2013).
[67] J. V. Moloney, J. Hader, and S. W. Koch, Laser Photonics Rev. **1**, 24 (2007).
[68] B. Guzelturk, M. Pelton, M. Olutas, and H. V. Demir, Nano Lett. **19**, 277 (2019).